SIRT5 Functions as a Tumor Suppressor via Reversing Warburg Effect in Renal Cell Carcinoma

Liu Yihan
Yale University
Wang Xiaojing
Shanghai Jiaotong University
Liu Ao
Shanghai Jiao Tong University School of Medicine
Zhang Chuanjie
Shanghai Jiaotong University: Shanghai Jiao Tong University
Wang Haofei
Shanghai Jiaotong University: Shanghai Jiao Tong University
Shen Yan
Shanghai Jiaotong University: Shanghai Jiao Tong University
Hongchao HE (hhc11775@rjh.com.cn)
Shanghai Jiaotong University: Shanghai Jiao Tong University https://orcid.org/0000-0003-4225-1142

Research Article

Keywords: SIRT5, Desuccinylation, PDHA1, Warburg effect, Renal cell carcinoma

Posted Date: August 20th, 2021

DOI: https://doi.org/10.21203/rs.3.rs-781256/v1

Abstract

Background: The aim of this study is to investigate the biological functions and the underlying mechanisms of SIRT5 in clear cell renal cell carcinoma (ccRCC).

Methods: The datasets of SIRT5 expression in The Cancer Genome Atlas Kidney Clear Cell Carcinoma (TCGA-KIRC) was selected and the correlation between SIRT5 and various clinicopathological parameters was analyzed. The SIRT5 expression in RCC tissues was examined by immunohistochemistry. The SIRT5 knockdown cell lines were constructed. *In vitro* and *in vivo* experiments were carried out to investigate the function of SIRT5 on cellular biology of RCC, including cell viability assay, wound-healing assay, soft agar colony formation assay, Transwell invasion assay, qRT-PCR, Western blot, etc. Besides, microarray, rescue experiment and Western blot were used to investigate the molecular mechanisms underlying the functions of SIRT5.

Results: SIRT5 expression was downregulated in RCC tissues, and low expression of SIRT5 was correlated with poor prognosis of RCC. Knockdown of SIRT5 significantly prompted cell proliferation, migration, and facilitated invasion *in vitro*. *In vivo* experiments revealed that knocking down SIRT5 prompted ccRCC tumorigenesis and metastasis. SIRT5 deglycosylated PDHA1 at K351 and increased the activity of PDC, thus changing the metabolic pathway to the TCA cycle and inhibiting the Warburg effect. The overexpression of SIRT5 was related to the low succinylation of PDHA1.

Conclusion: SIRT5 correlated with PDHA1 hyposuccinylation and progression in ccRCC, which suggested that SIRT5 might become a potential target for ccRCC therapy.

1. Background

Renal cell carcinoma (RCC) is one of the most aggressive malignancy of the urinary system, and its morbidity has increased gradually in the past few years. According to the USA cancer statistic data, 65000 newly diagnosed cases and approximately 15000 death were reported annually [1]. Clear cell renal cell carcinoma (ccRCC), accounting for > 80% histopathological type of sporadic RCC, was demonstrated to be associated with worse survival outcomes compared with other subtypes [2]. Metastatic ccRCC has a poor prognosis, and the 5-year overall survival (OS) rate is about 10%, while the 5-year OS rate of surgical-treated stage I ccRCC is over 90% [3]. Although combination strategies including surgery, targeted therapy, and immunotherapy have been optimized for the treatment of ccRCC, the clinical efficiency still improved marginally, especially in metastatic ccRCC [4]. Therefore, investigations on the detailed molecular mechanisms behind the tumorigenesis of ccRCC and the novel strategies are urgently required.

Tumorigenesis dependents on the reprogramming of cellular metabolism, which permits sustained biomass accumulation and redox homeostasis from a frequently nutrient-poor environment [5]. Cancer cells primarily utilize glycolysis for energy generation even in oxygen-rich conditions, this phenomenon is known as the Warburg effect, a metabolic hallmark of cancer [6]. Pyruvate, the end product of glycolysis, is transformed into lactate in cytoplasm or transported into mitochondria and catalyzed by pyruvate

dehydrogenase complex (PDC), providing acetyl-CoA and NADH for the TCA cycle and biosynthetic processes [7–13]. PDC was also reported to translocate into nucleus and generate acetyl-CoA for histone acetylation [14]. Eukaryotic PDC is composed of pyruvate dehydrogenase (E1), dihydrothioamide acetyltransferase (E2) and dihydrothioamide dehydrogenase (E3) [7]. Eukaryotic cells evolved strategies to regulate protein activity through post-translational modification, such as phosphorylation, acetylation, succinylation and so on [15–20]. The activity of PDC depends on the typical phosphorylation state of PDHA1, which is phosphorylated by pyruvate dehydrogenase kinase (PDK) 1–4 and dephosphorylated by pyruvate dehydrogenase phosphatase (PDP) 1–2 [10–12].

It was reported that SIRT3 deacetylated PDHA1 at the K321 and recruited PDP1 and finally increased PDC activity [21–22]. Another mitochondrial SIRT4 can hydrolyze the lipoamide cofactor from the E2 component dihydrolipoyllysine acetyltransferase (DLAT) and reduce PDH activity [23]. Recently, it was found that SIRT5, one of the three mitochondria sirtuins, could desuccinylate kinds of proteins, such as PDHA1 and SHDB, and regulates the activity of these proteins [20, 24]. However, the relationship between SIRT5 and cancer metabolism in ccRCC remains elusive. In this study, we aimed to investigate the expression and potential role of SIRT5 in ccRCC.

2. Methods

2.1 Patient samples

This study was approved by the Ethics Committee of Shanghai Ruijin Hospital, and all patients have provided written informed consent. ccRCC specimens (n = 280) histopathologically confirmed by three independent pathologists were made into a tissue microarray with matched normal sections. Six paired tumor and adjacent normal tissues were also obtained from ccRCC patients underwent radical nephrectomy in our institution. Clinical information was obtained from the medical records, including age, gender, tumor size, grade, stage. Tumor samples and adjacent normal tissues were placed into liquid nitrogen followed by storage at -80℃. In addition, computed tomography (CT) guided biopsies were collected from two ccRCC patients, and the patient derived organoids (PDO) were established and cultured.

2.2 Cell culture, materials and antibodies

HEK293T cells (ATCC CRL-11268) were cultured in DMEM (Gibco 12430-054) containing 10% FBS (Gibco 10099141), HeLa cells (ATCC CCL-2) and KMRC-20 cells (JCRB JCRB1071) were cultured in MEM (Gibco 11095-080) containing 1% NEAA (Gibco 11140-050) and 10% FBS, and Caki-1 cells (ATCC HTB-46) were cultured in McCoy 5'A (Gibco 11095-098) containing 10% FBS, RENCA cells (ATCC, CRL2947) were cultured in DMEM with 10%FCS (Gibco 10500-064). Cells were transfected with plasmids using Lipofectamine® 2000 Transfection Reagent (Thermo Fisher Scientific Cat. No: 12566014). Wild type SIRT5, SIRT5$^{\Delta 50}$ (lack the mitochondrion signal peptide, 1–36 AAs), wild type PDHA1, PDHA1 mutants were cloned into pcDNA3.1-Flag, pcDNA3.1-Myc and pcDNA3.1-HA vectors, respectively. The sequence of SIRT5 specific shRNA (5'-GCTGGAGGTTATTGGAGAA-3', 5'-CAGCATCCCAGTTGAGAAA-3') was used to

knock down of SIRT5 and the non-silencing shRNA oligonucleotide was used as a negative control. Anti-pan-succinyllysine antibody and anti-succ-K351 of PDHA1 were homemade. The synthetic PDHA1 peptides containing succinylated K351 was used as antigens to immunize rabbits and the purified serum proteins were measured. Antibodies specific to pyruvate dehydrogenase E1-alpha subunit antibody (Abcam), SIRT5 (Sigma), β-actin (Genscript), Flag-Tag (Abmart), Myc-Tag (Abmart), HA-Tag (Cell Signaling Technology), Mitochondria (Abcam) were purchased. PDH activity was determined using PDH Enzyme Microplate Assay Kit (Abcam ab109902).

2.2 In Vitro Succinylation and Desuccinylation

To succinylate the lysines containing peptides (GL Biochem), 0.5 mM Succinyl-CoA (Sigma) and 50 ng/μl peptides were mixed in 30 mM HEPES (pH 7.4) in a 15 μl system and kept at 37 ℃ for 3 hours. The peptides were desalted using C18 ZipTip (Millipore) prior to MALDI-TOF MS analysis. The desuccinylation was carried out by incubating enzymes with SIRT5 (Sigma) at 37℃ for 3 hours in 30mM HEPES buffer (6 mM $MgCl_2$, 1 mM DTT, 1 mM NAD^+, pH 7.4).

2.3 Animal Studies

Four-week-old male nude BALB/c mice obtained from Shanghai Lingchang Biotechnology Co., Ltd. were used to establish orthotopic tumor model. Mice had ad libitum access to a standard diet and water. Cages were maintained in well-ventilated racks in temperature and humidity controlled environment with a 12 h light/dark cycle. All animal experiments were approved by our institution Animal Research Ethics Committee. Luciferase-expressing Renca cells (1×10^5) stably transfected with shCtrl or shSIRT5 in 25 μL of 2:1 (v/v) PBS:Matrigel were injected into the sub-renal capsule of right kidney of BALB/c mice (5 mice/group). In vivo bioluminescence imaging (BLI) was performed to record the growth of tumor every 5 days and Living Image® software was used to quantify BLI signal. Mice were euthanized under anesthesia 28 days after implantation, tumor samples were fixed with 4% paraformaldehyde overnight, embedded in paraffin, and cut into 4 μm paraffin sections for subsequent experiments.

An in vivo lung metastasis model was generated using male nude BALB/c mice aged 4 weeks by the tail vein injection of Luciferase stable-expressing Caki-1 cells. Lung metastatic progression was monitored using the IVIS-100 system (Caliper Life Sciences). In vivo BLI were performed every 7 days and Living Image® software was used to analyze the data. Mice were euthanized 28 days after implantation, and lung metastatic lesions were analyzed by BLI system.

2.4 Western blot analysis

Western blot analysis followed standard procedures. After cell harvest, protein concentration was determined using Quantity One software (Bio-Rad, Hercules, Calif., USA). Cell lysate were separated by 10% SDS-Page, transfer to PVDF membranes (Millipore, Bedford, MA, USA) and blocked with 5% w/v skim milk for 2 hours at room temperature. Anti-PDHA1, Succ-K351 PDHA1, SIRT5, GAPDH, Actin antibody were incubated overnight at 4℃. Immune complexes were detected with horseradish peroxidase-conjugated secondary antibody (1:3000, Southern Biotech) for 2 hours at RT. Finally, they were visualized

using an enhanced chemiluminescence system (ECL; Pierce Company Woburn, MA, USA). Western blot signals were obtained by detecting chemiluminescence on Typhoon fla9500 (GE Healthcare). ImageJ (NIH) was used to analyze the densities of the bands. Each blot shown in the figures is representative of at least three experiments.

2.5 Immunofluorescence analysis

Standard procedures were followed for immunofluorescence analysis. Cells were seeded in 24-well plates, fixed with 4% paraformaldehyde, and then permeabilized with 1% Triton. Cells were incubated overnight at 4 ℃ with anti-PDHA1 and SIRT5 antibodies and detected the next day with Alexa-Fluor555 goat anti-mouse IgG antibody. The nuclei were stained with DAPI (Sigma). Immunofluorescence images were observed on a fluorescence microscope (Leica, DMI4000B).

2.6 Measurement of the activity of PDHA1 complex

PDHA1 activity was measured in a reaction buffer containing 50 mM KH2PO4 (pH 7.0), 1 mM MgCl2, 2 mM sodium pyruvate, 0.2 mM thiamine diphosphate and 0.1 mM 2,6- dichlorophenolindophenol (2,6-DCPIP). Purified PDHA1/PDHB complex was added to start the reaction. The reaction was maintained at 30 ℃. The course of the reaction was monitored by measuring the reduction of 2,6-DCPIP at 600 nm on a Roch spectrophotometer.

2.7 Oxygen Consumption Rates (OCR)

KMRC-20 cells or Caki-1 cells were seeded on XFe24 cell culture microplates (Seahorse Biosciences) at rates of 40000 or 15000 cells/well, respectively. The analysis was performed using the XF cell Mito stress test kit (Seahorse Bioscience) according to the manufacturer's protocol. Culture medium were replaced with the assay medium (XF Base Medium containing 5.5mM glucose, 2mM glutamine, 1% FBS, 1nM insulin, 100nM dexamethasone, pH7.4) (Seahorse Bioscience) 1 hour before analysis. Oligomycin, FCCP, Rotenone and Antimycin A used in assays were at final concentrations of 2 μM, 1 μM, 1 μM and 1 μM, respectively. The results were normalized by cell numbers.

2.8 Measurement of the growth curves

PDHA1 knockout cell were transfected with SIRT5, PDHA1, PDHA1 + SIRT5, PDHA1^{K351Q} or PDHA1^{K351Q} + SIRT5, respectively, and seed in 96-well plates. Cell morphology was observed under an inverted microscope, the plate and its contents were allowed to equilibrate at room temperature for about 30 minutes, a transparent bottom was affixed with a white back cover, and the luminescence was recorded with EnSpire.

2.9 Soft agar colony formation assay

For soft agar colony formation assays, a base of 2 ml of medium containing 10% FBS with 0.7% agar was used. Cells were seeded in 2 ml of medium containing 10% FBS with 0.35% agar at the density of 1×10^5 cells per well and incubated for 21 days at 37 ℃. Then, the number of colonies developed in soft agar was counted using Image J, and images were taken under an Olympus IX5 microscope.

2.10 Wound-healing assay

Cell migration ability was assessed by a wound-healing assay. Briefly, Caki-1 cells were transfected with PDHA1, PDHA1 + SIRT5, PDHA1^{K351Q} or PDHA1^{K351Q} + SIRT5, respectively. Approximately 5×10^6 cells were seeded into 24-well plates and cultured for 24 hours. Then a yellow plastic pipette tip was used to create a wound by scraping the cells. Cell migration was monitored under Nicon Eclipse microscope and photographed at 100×.

2.11 Transwell invasion assay

Cell invasion experiments were carried out using 24-well Transwell plates with 8 μm pore polycarbonate Matrigel-coated membrane inserts according to the manufacturer's instruction. After 20 h of incubation, non-invading cells in the upper insert were removed and cells that had invaded into the lower matrigel surface were fixed with 4% paraformaldehyde, stained with 0.5% crystal violet, and 10 random fields of view were quantified.

2.12 Immunohistochemistry

Formalin-fixed and paraffin-embedded specimens were prepared for histological section. Antigen recovery was performed on renal carcinoma specimens incubated with Tris-EDTA buffer (ph8.4) at 99 ℃ for 60 minutes. Endogenous peroxidase was inactivated in methanol and 3% H_2O_2 solution. Slides were incubated with primary antibody for 60 minutes, secondary antibody for 8 minutes, and DAB developer for 8 minutes. All procedures were performed using the Ventana BenchMark XT automated stainer and the slides were scanned by Ventana iScanCoreo scanner. Quantification of IHC results was performed by experienced pathologists. The intensity was calculated according to the positive area and the positive degree. The sections were stained with SIRT5 (1:100), PDHA1 (1: 100), Succ-K351-PDHA1 (1: 100) and Ki67 (1: 100) antibodies using ultraView Detection Kit.

2.13 Statistical analysis

Data were expressed as the mean ± standard deviation (SD), and bars in the graph represent standard deviation. Statistical analyses were conducted using SPSS 22.0 software (IBM, Corp., Armonk, NY, USA). Significant differences between groups were determined using Student's T test. The significance level for statistical testing was set at $P < 0.05$.

3. Results

3.1 SIRT 5 is downregulated and associated with prognosis in ccRCC patients

The RNA-seq datasets and clinical information of ccRCC patients were downloaded from The Cancer Genome Atlas (TCGA; https://portal.gdc.cancer.gov/). We performed a comprehensive bioinformatics analysis and found that SIRT5 expression was significantly lower in ccRCC tissues compared with normal tissues ($P = 8.308e^{-16}$) (Fig. 1A). We further detected the expression of SIRT5 in 72 paired ccRCC tumor samples and paracancerous normal tissues and found that SIRT5 was significantly decreased in the tumor samples (P = 4.117e-09) (Fig. 1B). In addition, ccRCC patients in TCGA-KIRC cohort with lower SIRT5 expression level had higher clinicopathological TNM stage and grade (Fig. 1C-G). Kaplan-Meier analysis verified that patients with lower SIRT5 levels had a worse overall survival prognosis (Fig. 1H). We then performed SIRT5 gene cluster analysis of different ccRCC samples by WGCNA and found the correlation coefficient between SIRT5 and ccRCC was 0.236 ($P = 0.0002$) with a threshold of 12 (Figure I-K). GO functional enrichment analysis indicated that SIRT5 was primarily related to mitochondrial respiratory chain complex assembly and MAP2K/MAPK activation (Fig. 1L). KEGG pathway analysis also showed that the SIRT5 participated in fatty acid metabolism pathway and propionic acid metabolism pathway (Fig. 1M). These data indicated that SIRT5 might be involved in tumorigenesis of ccRCC by regulating cancer metabolism.

3.2 SIRT5 desuccinylates PDHA1

It was found that wild type SIRT5 decreased the pan-succinylation of PDHA1 (Fig. 2A), which suggested the activity of PDC might be regulated by SIRT5. To test this hypothesis, we first analyzed the interaction between SIRT5 and PDHA1. SIRT5 was co-purified with PDHA1 and PDHA1 was also co-purified with SIRT5, when they are co-expressed in HEK293T cells (Fig. 2B&C), suggested that SIRT5 and PDHA1 could interact with each other. Incubation of recombinant PDHA1 (rPDHA1) with succinyl-CoA resulted in a gradual increase of the succinylation levels of PDHA1 in a succinyl-CoA-dependent manner (Fig. 2D), confirmed that PDHA1 could be succinylated directly. Moreover, it was found that overexpression of SIRT5 removed the succinylation of PDHA1 in SIRT5 stably expressed cell line (Fig. 2E) and knockdown of SIRT5 could increase the PDHA1 succinylation (Fig. 2F). These data suggested that SIRT5 contributes to the desuccinylation of PDHA1.

3.3 SIRT5 desuccinylates K351 of PDHA1

To determine which lysine sites of PDHA1 were desuccinylated by SIRT5, we mutated each candidate lysine sites of PDHA1 according to the previously published data [15, 18]. It was found SIRT5 had no effect on the K77, K121 and K374 of PDHA1, but desuccinylated the K351 of PDHA1 (Fig. 3A), suggested that K351 of PDHA1 might be the substrate of SIRT5. Interestingly, SIRT5 only decreased the succinylation of wild type PDHA1, but not its desuccinylation mimetic K351R or succinylation mimetic K351Q mutants, indicated that K351 might be the substrate of SIRT5 (Fig. 3B). To verify that K351 of PDHA1 is the substrate of SIRT5, we generated site-specific antibodies against Succ-K351 of PDHA1 by employing synthetic succinylated PDHA1 peptides as antigens (Fig. 3C). The levels of Succ-K351 of endogenous PDHA1 were measured under SIRT5 overexpression and knockdown conditions to test whether SIRT5 desuccinylated endogenous PDHA1. To exclude a potential effect of endogenous PDHA1,

PDHA1 were knocked down and then re-introduced into the HEK293 cell line. The results demonstrated that SIRT5 decreased the K351 succinylation of wild type PDHA1, but had no effect on the K351 mutants (Fig. 3D). Overexpression of wild type SIRT5 in HeLa cells decreased the levels of endogenous Succ-K351 of PDHA1; however, overexpression of the mitochondria localization defective but functional mutant ($SIRT5^{\Delta 50}$) failed to do so (Fig. 3E). Conversely, knocking down SIRT5 increased the level of Succ-K351 on endogenous PDHA1 (Fig. 3F). These results collectively supported that K351 of PDHA1 might be the desuccinylation site of SIRT5.

3.4 SIRT5 desuccinylates PDHA1 and regulates metabolic pathways

To confirm that SIRT5 desuccinylates PDHA1 and reroutes the metabolic pathways, we first test the effect of succinyl-CoA on the succinylation and the activity of PDHA1. It was found that succinyl-CoA increased the succinylation of PDHA1, but decreased its activity (Fig. 4A). Then the succinylation of PHDA1 and the activity of PDHA1 under conditions of SIRT5 overexpression or knockdown were evaluated. It was observed that overexpression of SIRT5 decreased the succinylation of PDHA1 but increased its activity (Fig. 4B). Conversely, knocking down SIRT5 increased PDHA1 succinylation and decreased its activity (Fig. 4C).

We further evaluated the OCR and metabolites of glycolysis and TCA cycle to confirm the rerouting metabolic pathways by SIRT5. It was found that the OCR of KMRC-20 cells were decreased by 5mM DMHG treatment, but overexpressing SIRT5 rendered the OCR of KMRC-20 cells resistant to DMHG (Fig. 4D), suggested that SIRT5 could regulate the OCR of KMRC-20 cells. It was also found that knocking down SIRT5 decreased the OCR of Caki-1 cells (Fig. 4E). Moreover, we analyzed the metabolites of glycolysis and TCA cycle and found that SIRT5 decreased the concentration of glucose-6-phosphate (G6P), 3-phosphoglyceric acid (3-PG), pyruvate and lactate level and increased citrate level (Fig. 4F), demonstrated that SIRT5 decreased glycolysis and increased TCA cycle.

Lastly, overexpression of SIRT5 dramatically decelerated Caki-1 proliferation, whereas knocking down SIRT5 significantly promoted Caki-1 proliferation (Fig. 5A). Knocking down PHDA1 in Caki-1 increased its proliferation, but when re-introduced both of PDHA1 and SIRT5, the cell proliferation decreased significantly (Fig. 5B). Interestingly, overexpression of $PDHA1^{K351Q}$ increased the proliferation of Caki-1 cells, and SIRT5 has no effect on this cell line. It was also found that knockdown of SIRT5 significantly promoted proliferation, migration, and SIRT5 inhibited cell migration through PDHA1, but could not reverse $PDHA1^{K351Q}$-mediated increased cell migration (Fig. 5D & 5E). At the same time, ccRCC organoid models was established to confirm the potential clinical value of SIRT5. The results revealed that knockdown of SIRT5 significantly increased cell proliferation in the PDOs generated from two different ccRCC patients (Fig. 5C). These results supported the hypothesis that desuccinylation of PDHA1 by SIRT5 regulated the metabolic pathways and inhibited cell proliferation, migration and invasion in ccRCC.

3.5 SIRT5 correlates with PDHA1 hyposuccinylation and progression in ccRCC

Immunohistochemistry and Western blot assays were performed in 6 paired specimens in order to illustrate differential expression of each marker in normal and tumor tissues. SIRT5 was under-expressed in tumor tissues, alongside with elevated succinylation of K351 of PHDA1 in ccRCC (Fig. 6A&B). The results provided evidences that hypersuccinylation of PDHA1 promoted RCC disease progression, which could be reversed by overexpression of SIRT5. Immunohistochemical staining and statistical analysis in Ruijin-ccRCC cohort (n = 280) showed that the expression level of SIRT5 was significantly decreased in ccRCC samples than in normal tissues (Fig. 6C). The progression-free survival rate of patients with low SIRT5 expression was significantly higher than that of patients with high SIRT5 expression ($P < 0.05$) (Fig. 6D). The animal study showed the tumor size of the SIRT5-KO group was significantly larger than that in control group (Fig. 6F). HE staining and immunohistochemistry also showed that percentages of Ki-67 positive cells were apparently increased in SIRT5-KO group (Fig. 6E). We also found that knock down of SIRT5 significantly promoted metastatic processes compared with the control group in a lung metastasis model (Fig. 6G). These results suggested that SIRT5 played a suppressing role in the ccRCC tumorigenesis through regulating hyposuccinylation of PHDA1.

4. Discussion

Most cancer cells manifested an increased dependence on glycolysis to meet their energy demands, regardless of whether there is ample oxygen or not [6, 25]. PDC converts the pyruvate into acetyl-CoA and linked the glycolysis and TCA cycle [7–12]. Eukaryotic PDC is composed of E1, E2 and E3. Eukaryotic cells evolved hierarchical regulation strategies through post translational modification, such as phosphorylation [16], acetylation [16, 21], succinylation [17, 18, 22, 24], glutarylation [26], malonylation [19, 27], aminoacylations [28] and so on. And the PDC activity was reported to be regulated by the phosphorylation of PDHA1, which is phosphorylated by PDK1-4 and de-phosphorylated by PDP1-2 [6–13]. It was also found deacetylation of K321 of PDHA1 by SIRT3 increased its activity [19–20]. SIRT4, a mitochondria targeted sirtuin, could hydrolyze the DLAT and diminish the PDH activity [23]. PDC has been recently reported to translocate into nucleus and generate acetyl-CoA for histone acetylation [14], suggested the functions of PDC still needed to be investigated further.

SIRT5, one of the three mitochondria sirtuins, was reported to deacetylate and activate urate oxidase in liver mitochondria of mice [29], but SIRT5 was reported to mediated other protein post-translational modifications, such as desuccinylation [12, 13, 17, 19], glutarylation [26] and malonylation [19, 27]. It was reported that SIRT5 could desuccinylate and activate SOD1 to eliminate ROS [30]; dusuccinylate and activate PKM2 to block macrophage IL-1β production and prevent DSS-induced colitis [31]; desuccinylate and activate SHMT2 to drive cancer cell proliferation [32]. Recently, two papers published on Molecular Cell [20, 24] showed that SIRT5 desuccinylate PDHA1 and SHDB, but positively or negatively regulate the protein enzymatic activity. And it was found that SIRT5 promote melanoma cell survive partially through

PDC [33]. Although SIRT3 and SIRT4 acted as tumor suppressors, the relationship between SIRT5 and cell metabolism and cancer remain elusive. In this study, we found that SIRT5 desuccinylate the K351 of PDHA1 and increased its activity, thus increased the metabolic flow through TCA cycle and reverse Warburg effect (Fig. 7). We also found that SIRT5 desuccinylate PDHA1 and decreased its oxygen consumption, causing inhibition of cell proliferation and migration in ccRCC. Moreover, we observed that hyper-succinylation of PDHA1 related to disease progression in ccRCC and SIRT5 played a suppressing role in the ccRCC tumorigenesis through regulating hyposuccinylation of PHDA1. Notably, the molecular mechanisms underlying how desuccinylation of PDHA affects its enzyme activity remains unclear. Future research based on a more comprehensive study is needed to explore the underlying mechanism.

5. Conclusions

SIRT5 correlated with PDHA1 hyposuccinylation and progression in ccRCC, which suggested that SIRT5 might become a potential target for ccRCC therapy.

Declarations

Conflict of Interest

The authors declare that the research was conducted in the absence of any commercial or financial relationships that could be construed as a potential conflict of interest.

Author Contributions

YS and HH conceived and designed that study. YS, YL, XW, AL and CZ contributed to the experiment and analysis of the data. YL and XW wrote the first draft of manuscript. HW and HH critically revised the manuscript. All authors read and approved the final manuscript.

Funding

This study was supported by the Medical and Technology Intercrossing Research Foundation of Shanghai Jiaotong University (YG2016QN65) and the Guangci Excellent Youth Program of Ruijin Hospital (GCQN-2018-B15).

Acknowledgments

We thank Ms IVY (Shanghai Hover International Education & John Picture) for helping to create illustrations used in this study.

References

1. Barata, P.C. and B.I. Rini, Treatment of renal cell carcinoma: Current status and future directions. CA Cancer J Clin, 2017. 67(6): 507-524.

2. Hakimi, A.A., et al., Transcriptomic Profiling of the Tumor Microenvironment Reveals Distinct Subgroups of Clear Cell Renal Cell Cancer: Data from a Randomized Phase III Trial. Cancer Discov, 2019. 9(4): 510-525.
3. Mitchell, T.J., et al., Timing the Landmark Events in the Evolution of Clear Cell Renal Cell Cancer: TRACERx Renal. Cell, 2018. 173(3): 611-623 e17.
4. Ljungberg, B., et al., European Association of Urology Guidelines on Renal Cell Carcinoma: The 2019 Update. Eur Urol, 2019. 75(5): 799-810.
5. Pavlova, N.N. and C.B. Thompson, The Emerging Hallmarks of Cancer Metabolism. Cell Metab, 2016. 23(1): 27-47.
6. Warburg O. On the origin of cancer cells. Science. 1956. 123 (3191): 309-314.
7. Bowker-Kinley MM., et al. Evidence for existence of tissue-specific regulation of the mammalian pyruvate dehydrogenase complex. Biochem. J. 1998. 329: 191-196.
8. Patel MS. and Korotchkina LG. Regulation of mammalian pyruvate dehydrogenase complex by phosphorylation: complexity of multiple phosphorylation sites and kinases. Exp. Mol. Med. 2001. 33(4): 191-197.
9. CaJacob CA., Gavino GR. and Frey PA. Pyruvate dehydrogenase complex of Escherichia coli thiamin pyrophosphate and NADH-dependent hydrolysis of acetyl-CoA. J. Biol. Chem. 1985. 260(27): 14610-14615.
10. Kolobova, E., et al. Regulation of pyruvate dehydrogenase activity through phosphorylation at multiple sites. Biochem. J. 2001. 358: 69-77.
11. Kato M., et al. Structural basis for inactivation of the human pyruvate dehydrogenase complex by phosphorylation_role of Disordered phosphorylation loops. Structure. 2008. 16: 1849-1859.
12. Korotchkina LG. and Patel MS. Probing the mechanism of inactivation of human pyruvate dehydrogenase by phosphorylation of three sites. 2001. J. Biol. Chem. 276(8): 5731-5738.
13. Ciszak EM., et al. Structural basis for flip-flop action of thiamin pyrophosphate-dependent enzymes revealed by human pyruvate dehydrogenase. J. Biol. Chem. 2003. 278(23): 21240-21246.
14. Sutendra G., et al. A nuclear pyruvate dehydrogenase complex is important for the generation of acetyl-CoA and histone acetylation. Cell. 2014. 158: 84-97.
15. Shi YG. Serine/threonine phosphatases_ mechanism through structure. Cell. 2009. 139: 468-484.
16. Li XL. and Kazgan N. Mammalian sirtuins and energy metabolism. Int. J. Biol. Sci. 2011. 7: 575-587.
17. Rardin MJ., et al. SIRT5 regulates the mitochondrial lysine succinylome and metabolic networks. Cell Metab. 2013. 18: 920-933.
18. Du JT., et al. Sirt5 is a NAD-dependent protein lysine demalonylase and desuccinylase. Science. 2011. 334(6057): 806-809.
19. Peng C., et al. The first identification of lysine malonylation substrates and its regulatory enzyme. Mol. Cell. Proteomics. 2011. 10(12): M111.012658: 1-12. DOI: 10.1074/mcp.M111.012658.

20. Park J., et al. SIRT5-mediated lysine desuccinylation impacts diverse metabolic pathways. Mol. Cell. 2013. 50: 919-930.
21. Fan J., et al. Tyr phosphorylation of PDP1 toggles recruitment between ACAT1 and SIRT3 to regulate the pyruvate dehydrogenase complex. Mol. Cell. 2014. 53: 534-548.
22. Jing EX., et al. Sirt3 regulate metabolic flexibility of skeletal muscle through reversible enzymatic deacetylation. Diabetes. 2013. 63: 3404-3417.
23. Mathias RA., et al. Sirtuin 4 Is a lipoamidase regulating pyruvate dehydrogenase complex activity. Cell. 2014. 159: 1615-1625.
24. Li F., et al. $NADP^+$-IDH mutations promote hypersuccinylation that impairs mitochondria respiration and induces apoptosis resistance. Mol. Cell. 2015. 60: 661-675.
25. Hannahan D. and Weinberg RA. Hallmarks of cancer: the next generation. Cell. 2011. 144: 646-674.
26. Tan MJ., et al. Lysine glutarylation is a protein posttranslational modification regulated by SIRT5. Cell Metab. 2014. 19: 605-617.
27. Nishida Yuya., et al. SIRT5 regulates both cytosolic and mitochondrial protein malonylation with glycolysis as a major target. Mol. Cell. 2015. 59: 321-332.
28. He XD., et al. Sensing and transmitting intracellular amino acid signals through reversible lysine aminoacylations. Cell Metab. 2018. 27: 1-16.
29. Nakamura Y., et al. SIRT5 deacetylates and activates urate oxidase in liver mitochondria of mice. FEBS. Lett. 2012. 586: 4076-4081.
30. Lin ZF., et al. SIRT5 desuccinylates and activates SOD1 to eliminate ROS. Biochem. Biophys. Res. Commun. 2013. 441: 191-195.
31. Wang F., et al. SIRT5 desuccinylates and activates pyruvate kinase M2 to block macrophage IL-1β production and to prevent DSS-induced colitis in mice. Cell Rep. 2017. 19: 2331-2344.
32. Yang X., et al. SHMT2 desuccinylation by SIRT5 drives cancer cell proliferation. Cancer Res. 2018. 78(2): 372-86.
33. Park J., et al. Human melanoma cell need SIRT5 to survive. Free Radic. Biol. Med. 2016. 100: S128.

Figures

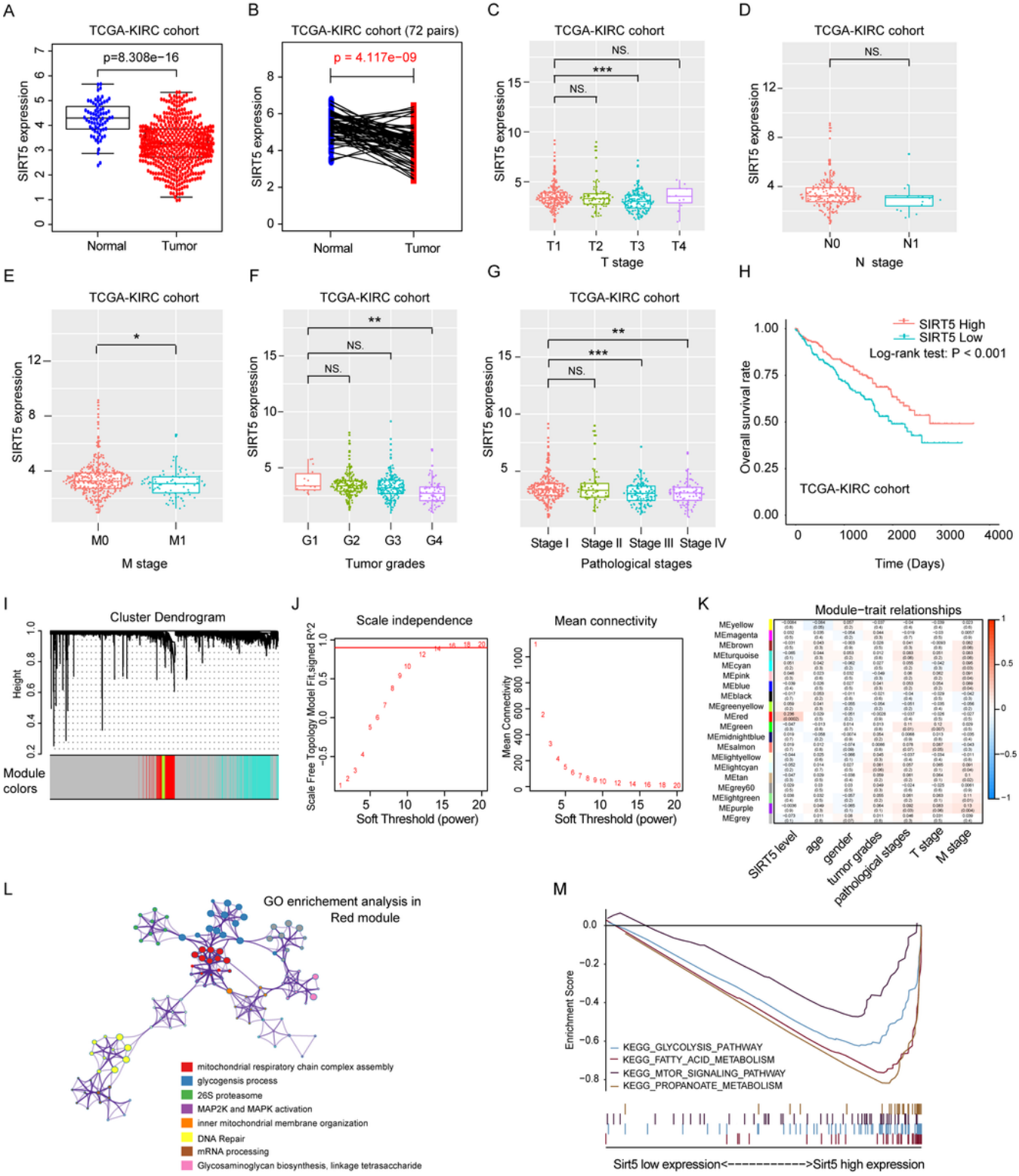

Figure 1

SIRT5 is downregulated and associated with prognosis in ccRCC patients. (A) SIRT5 expression in tumor and normal tissues in the TCGA-KIRC dataset. (B) SIRT5 expression in 72 paired ccRCC tissues from TCGA-KIRC cohort. SIRT5 expression levels were compared in different clinicopathological parameters: TNM stage (C-E), tumor grades (F) and pathological stage (G). (H) Kaplan–Meier analysis of OS stratified by SIRT5 expression in the TCGA-KIRC dataset. Cluster dendrogram (I), soft threshold (J) and Module-trait

relationship (K) were analyzed by WGCNA. (L) Go functional enrichment analysis. (M) KEGG pathway analysis.

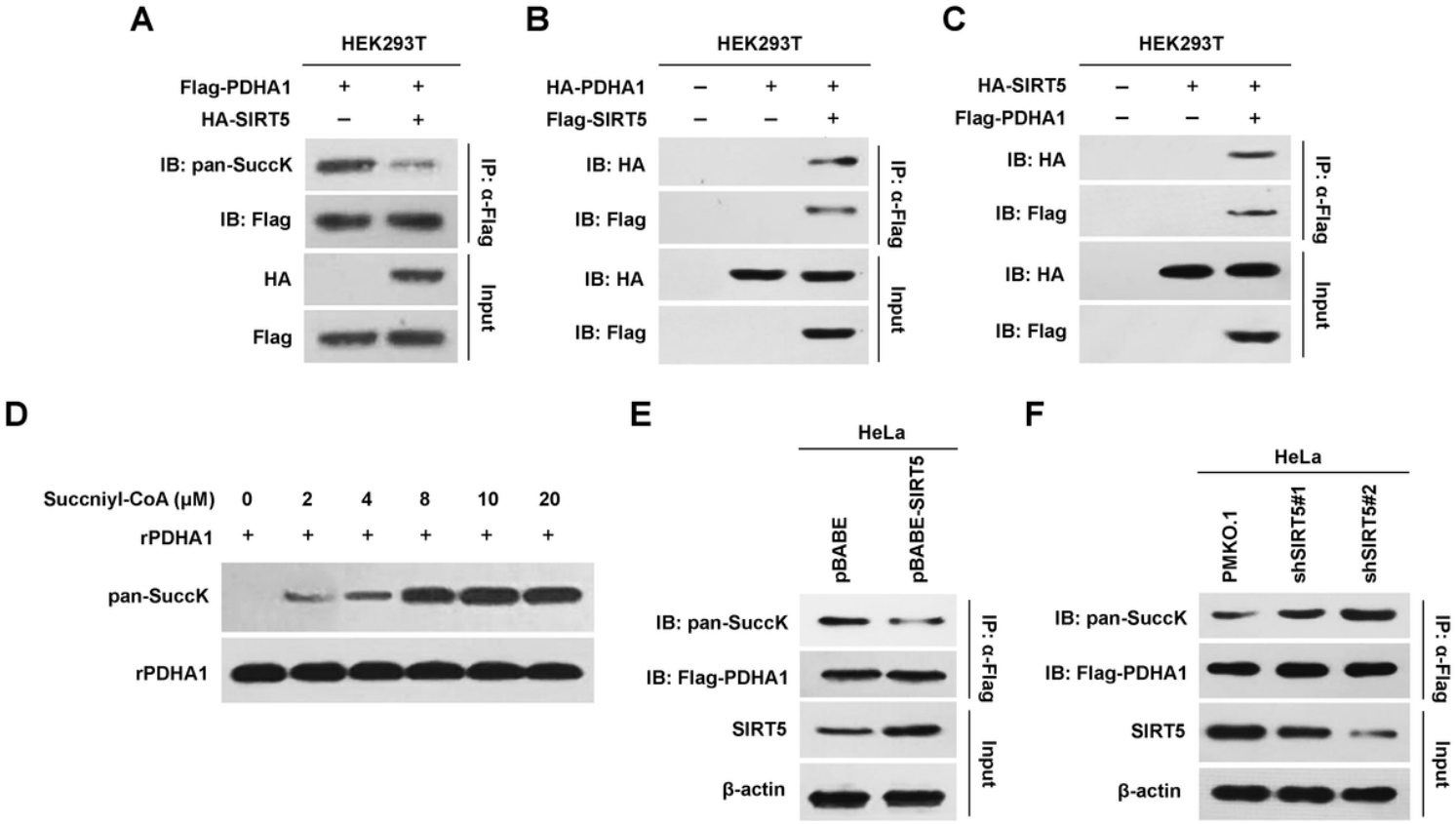

Figure 2

SIRT5 desuccinylates PDHA1. (A) Flag-PDHA1 and HA-SIRT5 were introduced into HEK293T cells and the pan-succinylation level of PDHA1 was determined. (B) HA-tagged PDHA1 and Flag-tagged SIRT5 were co-expressed in HEK293T cells. The PDHA1 co-purified with the SIRT5 was detected by HA antibody. (C) HA-tagged SIRT5 and Flag-tagged PDHA1 were co-expressed in HEK293T cells. The SIRT5 co-purified with the PDHA1 was detected by HA antibody. (D) Diluted succinyl-CoA was added into purified PDHA1 system and the pan-succinylation level of recombinant PDHA1 (rPDHA1) was determined. (E) pBABE-SIRT5 and control vector were introduced into HeLa cells and pan-succinylation of PDHA1 were determined. (F) SIRT5 was knocked down in HeLa cells and pan-succinylation of PDHA1 were determined.

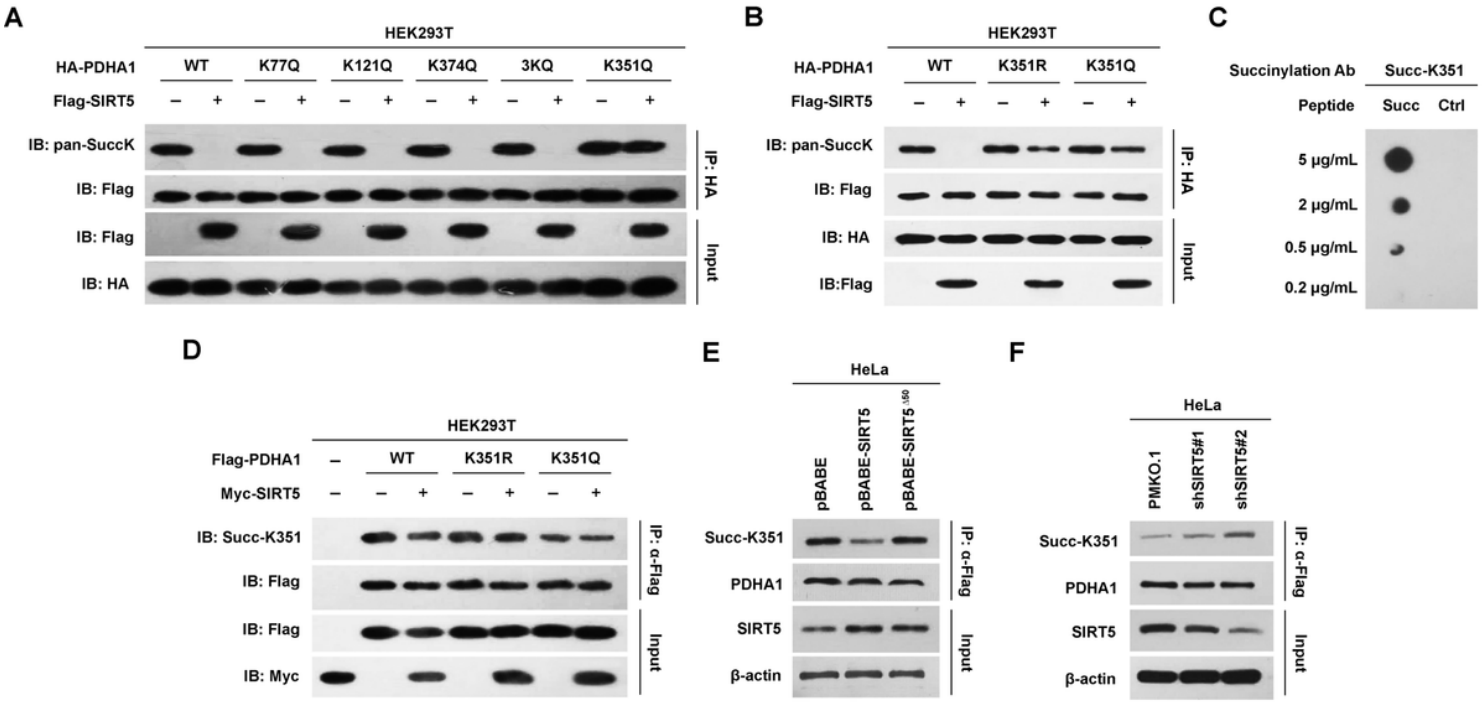

Figure 3

SIRT5 desuccinylates PDHA1 at K351. (A) Lysine 77 (K77), K121, K374, K351 and 3K (K77, K121 and K374) of PDHA1 were mutated into glutamine, respectively and introduced into HEK293T cells, then the pan-succinylation level of PDHA1 was determined under the presence or absence of SIRT5. (B) Lysine 351 (K351) of PDHA1 was mutated into arginine (R) and glutamine (Q), respectively and then introduced into HEK293T with or without SIRT5, and the pan-succinylation level of PDHA1 was determined. (C) Validation of Succ-K351 antibody. Succ-K351 represented the peptide containing succinylated K351 and flanking sequence. (D) K351R and K351Q of PDHA1 were introduced into HEK293T cells with or without SIRT5 and the succinylation level of PDHA1 was determined. (E) SIRT5Δ50 was introduced into the HeLa cells and the succinylation level of endogenous PDHA1 was determined. (F) The succinylation levels of endogenous PDHA1 in HeLa cells before and after SIRT5 knockdown by independent shRNAs were compared.

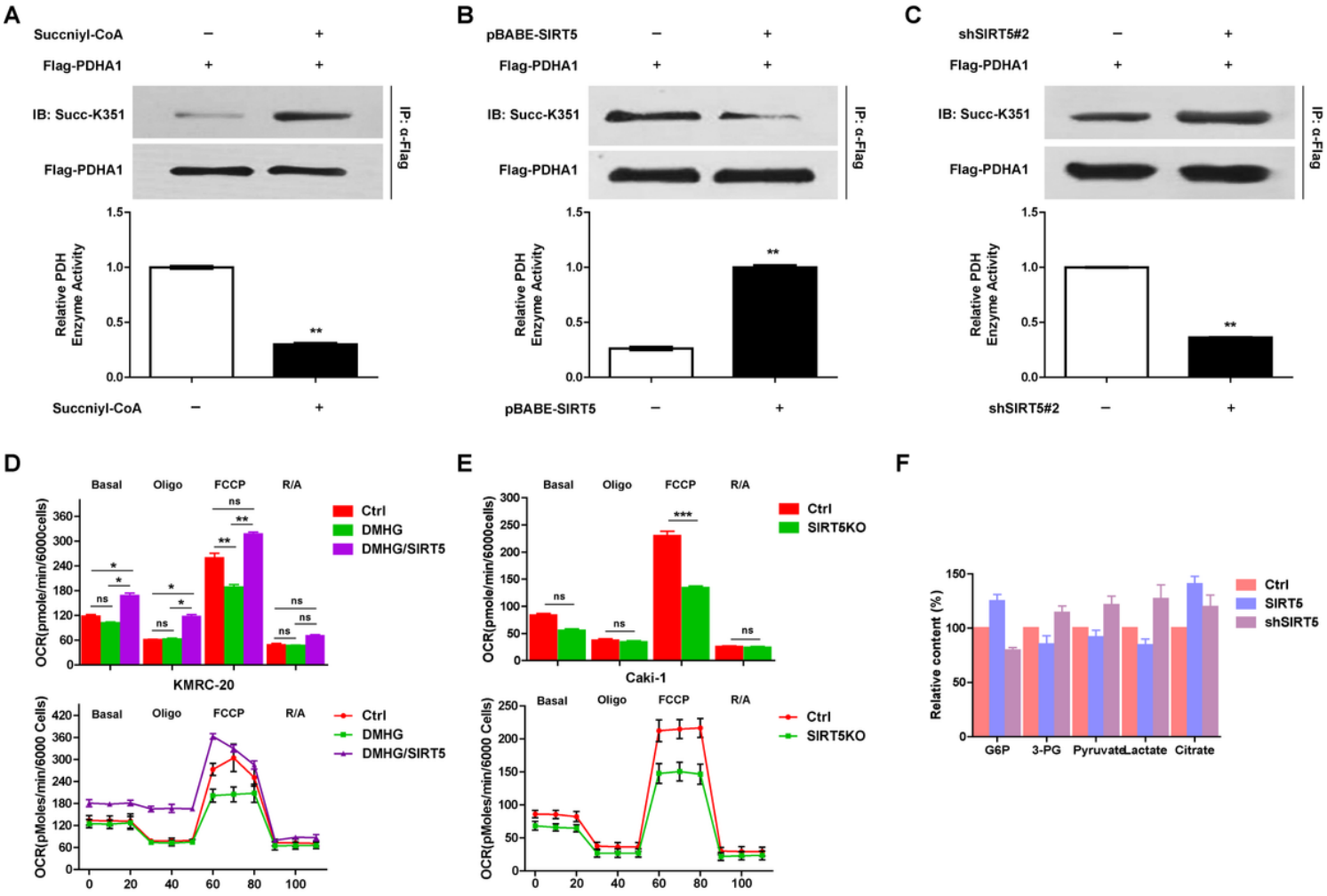

Figure 4

SIRT5 regulates PDHA1 activity and remodels the metabolic pathways. (A) Succinyl-CoA was added into the PDHA1 system and the succinylation level of PDHA1 and PDHA1 enzyme activity were determined. The succinylation level of PDHA1 and PDHA1 enzyme activity were determined under overexpression of PDHA1 (B) or knocking down PDHA1 (C). (D) OCR were detected for untransfected and SIRT5-transfected KMRC-20 that were treated by DMHG. OCR under oligomycin, carbonyl cyanide-m-chlorophenylhydrazone (FCCP), and antimycin A/rotenone treatments, respectively, at times indicated were obtained. (E) SIRT5 were knocked down in Caki-1 and the OCR were detected and quantified. (F) The key metabolites in glycolysis and TCA cycle were determined under overexpressing or knocking down SIRT5.

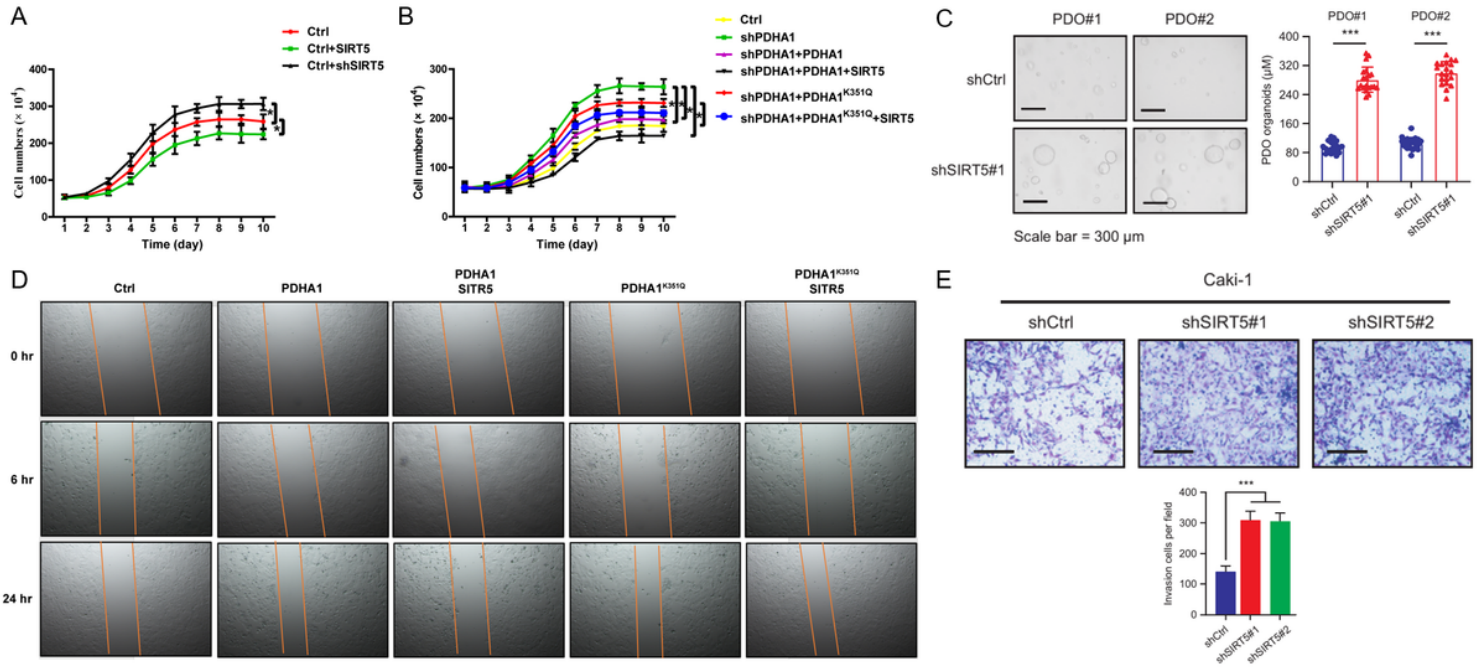

Figure 5

SIRT5 decelerates cell proliferation and inhibits cell migration through PDHA1. (A) Growth curves of overexpressed or knocking down SIRT5 in Caki-1 cells were determined. (B) PDHA1 was knocking down in Caki-1 cells and then the wild type and K351Q mutant (PDHA1K351Q) of PDHA1 were re-introduced into the cells, respectively. The growth curves of two modified Caki-1 cells with or without SIRT5 were compared. (C) Representative images of two different ccRCC organoids transfected with shCtrl or shSIRT5 lentivirus and quantification of organoid diameters. (D) Wild type and the mutant PDHA1K351Q of PDHA1 were introduced into Caki-1 cells and the photos of cells with or without SIRT5 were captured at 0, 6, and 24hrs. (E) Transwell invasion assay of wild type and shSIRT5 Caki-1 cells.

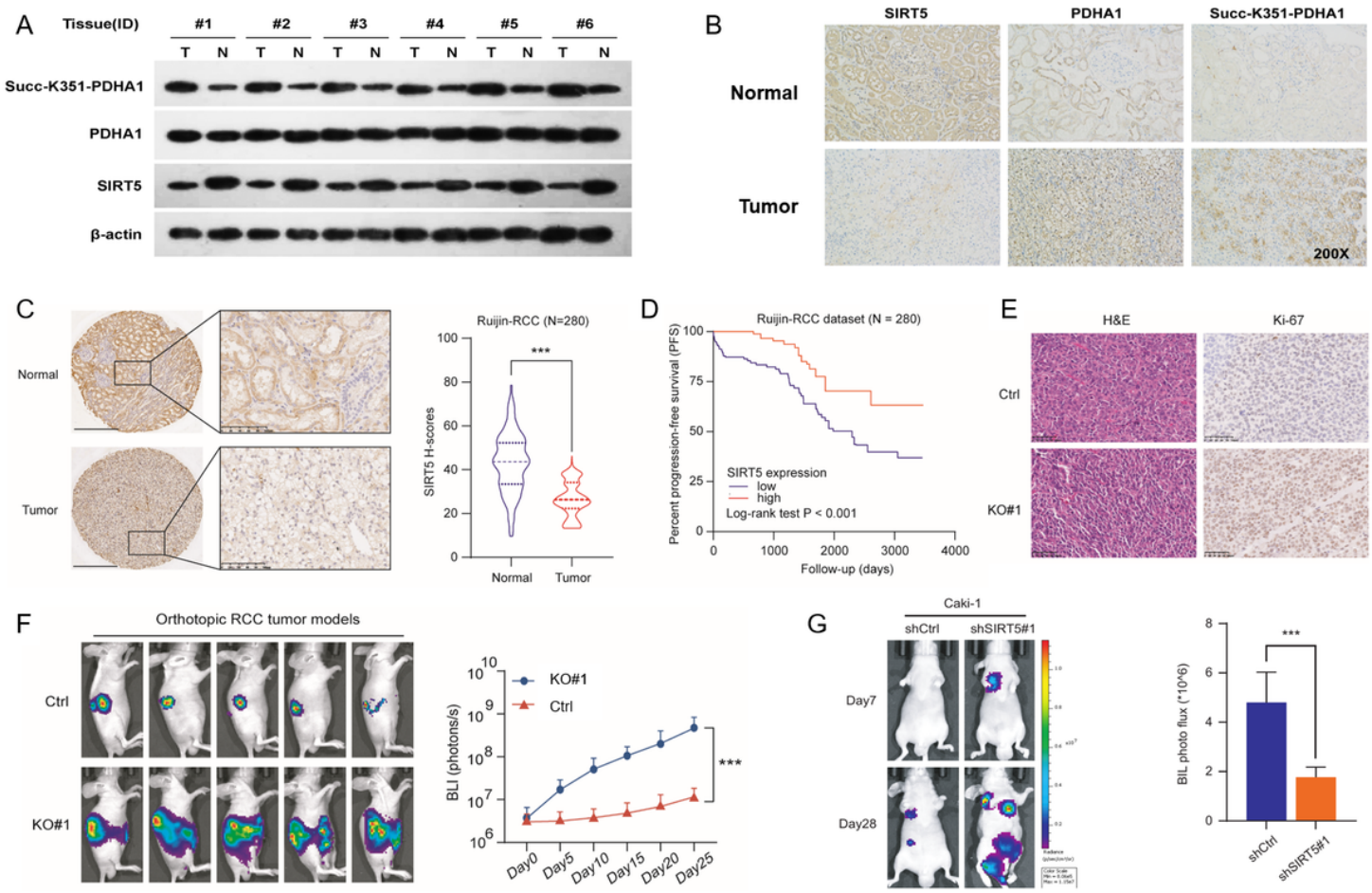

Figure 6

SIRT5 correlates with hyposuccinylation and progression in ccRCC. The succinylation levels of PDHA1 and SIRT5 were compared in 6 paired tumor and normal tissues by western blot (A) and immunohistochemistry (B). (C) Representative images of immunohistochemistry for SIRT5 protein in Ruijin-ccRCC dataset. SIRT5 expression in tumor and normal tissues in Ruijin-ccRCC dataset. (D) Kaplan–Meier analysis of PFS stratified by SIRT5 expression in Ruijin-ccRCC dataset. HE staining (E) and in vivo BLI (F) of an orthotopic model generated with WT and SIRT5-KO Luc-RENCA cells. (G) In vivo BLI of a lung metastasis model generated with WT and SIRT5-KO Luc-Caki-1 cells.

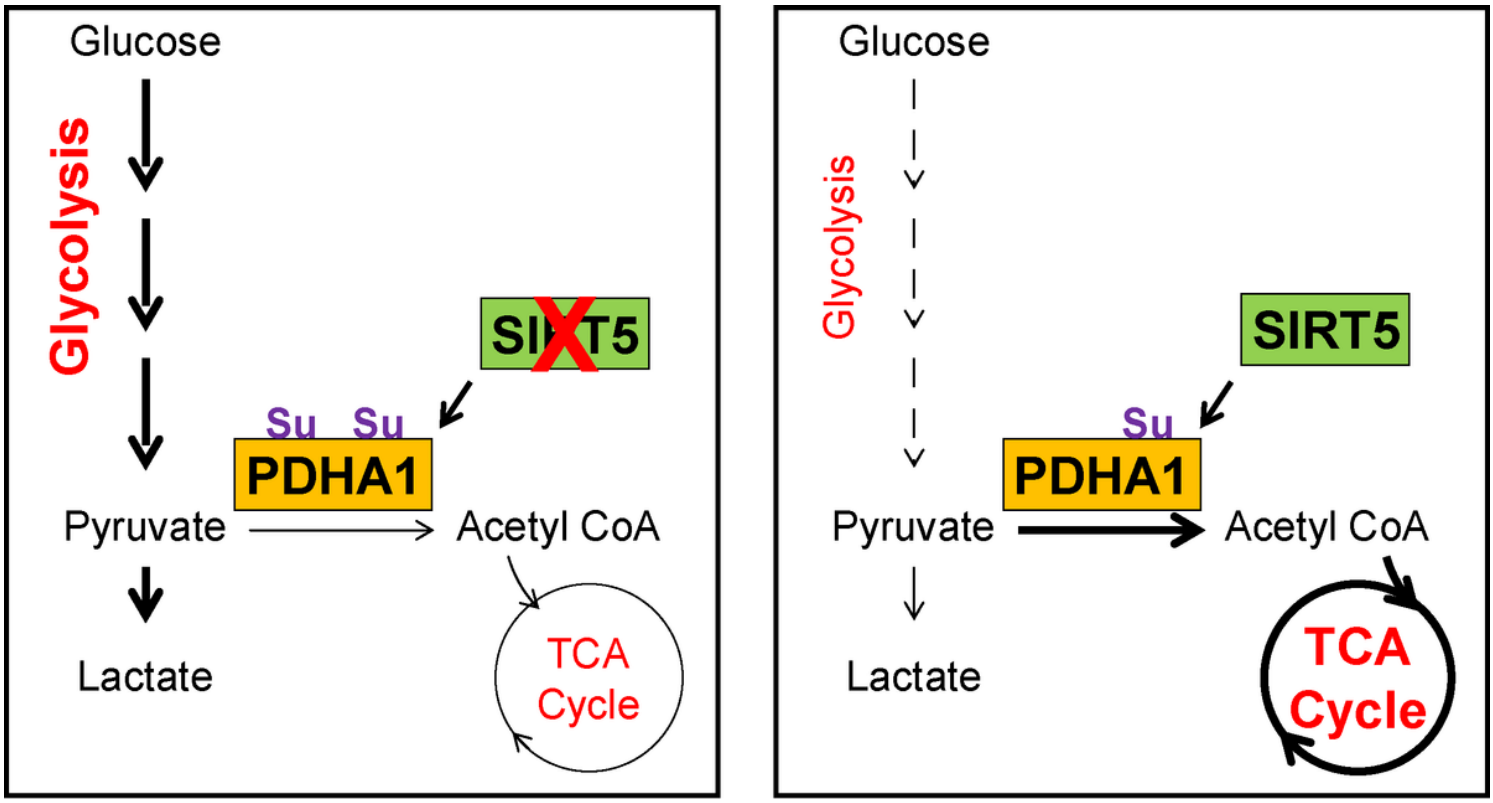

Figure 7

Schematic diagram of the proposed mechanism by which SIRT5 reversed Warburg effect.